GPS Solutions (2024) 28:195
https://doi.org/10.1007/s10291-024-01742-3

ORIGINAL ARTICLE

Chip-scale atomic clock (CSAC) aided GNSS in urban canyons

Yang Meng[1,2] · Duojie Weng[1,2,4] · Cheng Yang[3] · Wu Chen[2] · Zhiyu Hou[2]

Received: 19 June 2024 / Accepted: 30 August 2024

Abstract
In urban canyons, the reflections and obstructions of Global Navigation Satellite System (GNSS) signals frequently lead to significant errors in measurements, the number of which can be larger than that of the correct measurements. This leads to a severe degradation of GNSS performance in urban canyons. Various fault detection and exclusion (FDE) algorithms have been developed to cope with these outliers caused by multipath effects. Most of these FDE algorithms check the consistency among measurements. However, in urban canyons, their effectiveness is significantly compromised by the lack of fault-free measurements. There is an urgent need to develop new constraints for enhancing GNSS FDE performance. In recent years, the advent of Chip-Scale Atomic Clock (CSAC), known for their affordability and high frequency stability, offers a promising solution for accurately predicting receiver clock errors. Additionally, using city maps to establish height constraints is another way to increase redundancy. The purpose of this study is to improve the GNSS positioning accuracy in urban canyons with the aid of CSAC and city map data. A novel FDE algorithm is developed to search for positions through the constraints of height and receiver clock. Extensive tests were conducted in urban canyons to evaluate the performance of the system. Results showed that the positioning accuracy can be improved from tens of meters to less than 6 m.

Keywords GNSS · Chip-scale atomic clock (CSAC) · Urban canyons · Fault detection and exclusion (FDE)

Introduction

In recent years, the Global Navigation Satellite System (GNSS) has seen significant advancements, providing many more satellites available in sky. Concurrently, advancements in electronics have enabled the integration of compact and cost-effective GNSS receivers as a standard feature in smartphones. This has laid a foundation for various Location-Based Services (LBS) that are required by diverse applications in various sectors including from smart cities to autonomous driving (Sheta et al. 2018; Weng et al. 2024; Yan et al. 2019).

Although GNSS can provide accurate position, velocity, and time (PNT) information in open outdoor areas, its effectiveness is compromised in urban areas. Urban environments present unique challenges for GNSS performance due to factors such as signal obstruction, reflections, and multipath effects, all of which can degrade positioning accuracy (Groves 2011). Particularly, urban canyons represent the most challenging urban scenarios, where high-rise buildings and narrow streets significantly obstruct the transmission of direct line-of-sight signals.

Multipath signals arise when satellite signals follow multiple paths, including both direct and reflected routes, before reaching the receiving antenna. On the other hand, non-line-of-sight signals occur when obstacles like buildings and trees obstruct the direct signal path, causing the receiver to capture signals reflected or diffracted from nearby surfaces. In this study, multipath effects refer to errors caused by multipath and NLOS signals. Techniques such as differential correction and modelling have been extensively used

✉ Duojie Weng
wengduojie.lsgi@polyu.edu.hk

1 The State Key Laboratory of Satellite Navigation System and Equipment Technology, Shijiazhuang, China

2 The Hong Kong Polytechnic University, Hung Hom, Kowloon, Hong Kong

3 China University of Geosciences Beijing, Beijing, China

4 Guangdong Key Laboratory of Urban Informatics and Guangdong Laboratory of Artificial Intelligence and Digital Economy (SZ), School of Architecture & Urban Planning, Shenzhen University, Shenzhen, China

Published online: 10 September 2024

to various GNSS errors, including satellite-related errors, the ionospheric errors, and the tropospheric errors (Weng et al. 2023). However, these techniques could not mitigate the multipath effects because they vary significantly under different environments (Dirksen et al. 2019).

Extensive efforts have been dedicated to mitigating GNSS multipath effects. One approach involves hardware solutions. Using a choke antenna proves effective in reducing multipath interference and attenuating non-directed signals. Additionally, dual-polarized antenna designs, featuring two mutually perpendicular polarization directions, offer improved discrimination between multipath signals and direct-line signals, mitigating the impact of multipath errors (Miao et al. 2020). However, these hardware solutions may not be feasible for consumer electronics devices due to potential increases in cost and size.

Another method involves checking consistency among GNSS measurements (Hsu et al. 2017). This method, which can be implemented through software adjustments or algorithm updates, does not require additional hardware modifications. It offers a flexible solution that can be used in various environments. However, in urban canyons, where buildings obstruct GNSS signals from both sides of the street, resulting in predominantly along-street signal reception, these methods face challenges as the majority of measurements are prone to multipath effects (Liu et al. 2024; Weng et al. 2023b).

The GNSS multipath effects in urban areas are mainly caused by the blockage and reflections of buildings. The external information about these buildings, i.e., the 3D building model, has thus been explored to enhance the performance of GNSS in urban areas (Hsu et al. 2016). These methods can be summarized into two types: (1) shadow matching based on signal-to-noise ratio (H.-F. Ng et al. 2021b); (2) matching based on ranging signals. Shadow matching based on signal-to-noise ratio involves evaluating the visibility of each satellite at various candidate locations, comparing it with the carrier-to-noise ratio observation data, and matching to obtain the optimal position(Wang et al. 2013). This technique has shown excellent performance in determining the left and right sidewalks(Wang et al. 2014), and preliminary studies have confirmed that it can achieve an accuracy rate of about 89% (H.-F. Ng et al. 2021b). The matching method based on ranging signals calculates virtual observations based on the 3D model at each candidate location, compares them with the observation data, and identifies the candidate point that best matches the actual observation data with the virtual observation data (Ng et al. 2021b). In the absence of urban 3D building models, other sensors such as fisheye lenses and LiDAR can effectively detect satellite visibility, thus being used to identify LOS and NLOS signals. Urban GNSS positioning technology assisted by scene information has laid the theoretical foundation for improving the accuracy of GNSS positioning in urban environments. However, the current technology still has the following shortcomings: (1) poor performance in the along street direction; (2) it requires the calculation of visible boundaries or signal propagation paths, which demands high computational complexity; (3) high reliance on 3D building models (Groves and Adjrad 2019).

In recent years, the exploration of additional constraints has been used to enhance GNSS performance in urban environments. Prior research has demonstrated that imposing height constraints, which can be obtained from Digital Elevation Models (DEMs) or barometric readings, can bring improvements in GNSS accuracy (Massarweh et al. 2020; Wang et al. 2023). Moreover, our recent studies have demonstrated that sidewalk constraints can also be employed to enhance the positioning accuracy for pedestrians, particularly in cross-street directions (Sharma et al. 2019; Weng et al. 2023b). These constraints use the predictable nature of pedestrian movement on sidewalks to improve localization (Weng et al. 2024). However, sidewalk constraints are specifically tailored for pedestrian applications and are not applicable to vehicular navigation.

The receiver clock bias is an important parameter that needs to be estimated together with position parameters. The traditional GNSS receivers rely on internal quartz oscillators like temperature-compensated crystal oscillators (TCXOs), which exhibited low frequency stability and accuracy. Therefore, we need to estimate this parameter epoch by epoch. In recent years, the chip-scale atomic clocks (CSACs), are becoming smaller, more affordable and portable (Cash et al. 2018). They offer enhanced signal stability, improved tracking recovery, and increased immunity to interference, particularly advantageous in high-density urban environments (Kunzi and Montenbruck 2023; Yao et al. 2019). The stable and accurate timing of CSACs provides us an opportunity to improve GNSS performance in urban canyons (Krawinkel and Schön 2016; Martinez et al. 2023). In this study, both the receiver clock constraints and the height constraints will be used to enhance the GNSS accuracy in urban canyons.

This paper is organized as follows. Section Challenges of GNSS positioning in urban canyons describes the challenge of GNSS in urban canyons. Section CSAC Constraints" presents the property of CSAC. Section ;GNSS FDE with the aid of an Urban Map and a CSAC describes the new GNSS positioning algorithm under constraints of the receiver clock error and the height. Section Performance Evaluation evaluates the proposed system in urban canyons. Section Conclusions concludes the proposed system.

Challenges of GNSS positioning in urban canyons

A GNSS receiver determines a user position using various measurements, among which pseudorange is widely used. The linearized equation for pseudorange can be formulated as follows

$$\boldsymbol{l} = \boldsymbol{A}\boldsymbol{x} + \boldsymbol{\epsilon} \tag{1}$$

where $\boldsymbol{l}$ denotes the pseudorange measurement vector with a dimension of $n \times 1$; $\boldsymbol{A}$ is a matrix including unit line-of-sight vectors from satellites to the receiver, augmented by a column of ones; $\boldsymbol{x}$ is the unknown vector comprising of three position components and a component of the receiver clock error: $\boldsymbol{x} = [\Delta x, \Delta y, \Delta z, \Delta t_R,]^T$; $\boldsymbol{\epsilon}$ denotes the measurement error including multipath errors together with other errors.

The weighted least squares method is commonly used to estimate the four unknowns in (1):

$$\widehat{\boldsymbol{x}} = (\boldsymbol{A}^{\boldsymbol{T}}\boldsymbol{W}\boldsymbol{A})^{-1}\boldsymbol{A}^{T}\boldsymbol{W}\boldsymbol{l} \tag{2}$$

where $\boldsymbol{W}$ is a diagonal weighting matrix, with the diagonal elements being the inverse of variances. It can be seen from (2) that the estimation can be affected severely by faults due to multipath effects. They must be detected and excluded before they contribute to GNSS solutions. Two types of consistency checking algorithms have been developed to improve the performance of urban GNSS. One is the residual based method, and another one is the subset testing.

The residual based fault detection and exclusion (FDE) algorithms attempt to check the consistency of measurements. The test statistic used in these algorithms is given by

$$\mathrm{v} = \boldsymbol{l} - \widehat{\boldsymbol{l}} = (\boldsymbol{I} - \boldsymbol{S})\boldsymbol{\epsilon} \tag{3}$$

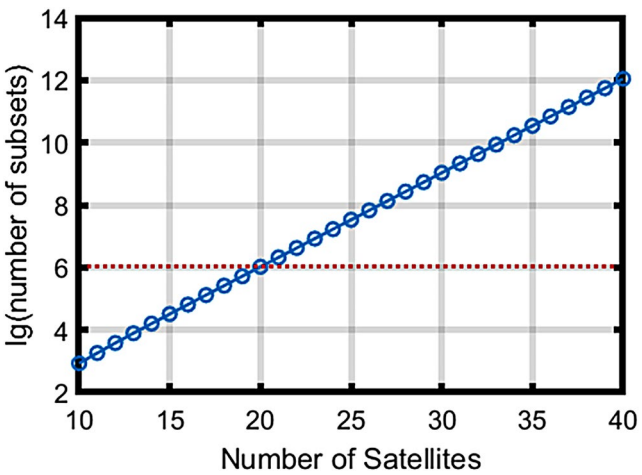

Fig. 1 The computational load vs. the number of observations in subset testing algorithm

where v is the residual; $\boldsymbol{I}$ is an identity matrix; $\boldsymbol{S} = \boldsymbol{A}\left(\boldsymbol{A}^{T}\boldsymbol{W}\boldsymbol{A}\right)^{-1}\boldsymbol{A}^{T}\boldsymbol{W}$. As shown, the residual is the product of the measurement errors $\boldsymbol{\epsilon}$ and the residual maker matrix $(\boldsymbol{I} - \boldsymbol{S})$. When there is only one or two faults, the use of the residual can detect and exclude these faults effectively. Nevertheless, when in case of multiple faults, the residual-based FDE approaches may result in the frequent exclusions of fault-free measurements and failures to detect faulty ones.

The subset testing algorithm is another consistency checking method that has been developed to cope with multiple faults. It involves mainly three steps: (1) selection of observation subsets; (2) fitting a model to each subset; and (3) finding the most consistent subset of observations. This method attempts to find the largest consistency among observation. Nowadays, tens of observations can be obtained from a multiple constellation GNSS receiver. The subset testing method requires a high computational load for the GNSS receiver. Figure 1 illustrates the relationship between the number of observations and the number of subsets that should be evaluated. As shown, computational complexity rises with the number of observations. For example, when the number of observations is 20, the number of subsets that needs to evaluated is as large as 1 million, as indicated by the red dashed line in the Fig. 1. For each subset, it is necessary to calculate the position, where both matrix multiplication and inversion need substantial computational resources.

More importantly, in urban canyons, tall buildings obstruct signals, leading to majority of the observable measurements being erroneous. The low observability to clear measurements significantly complicates the FDE process, making it challenging to achieve satisfactory results in urban canyons. Consequently, additional constraints are urgently required to enhance FDE performance and improve positioning accuracy.

CSAC constraints

GNSS technology determines positions by measuring the time differences between different satellite clocks and the receiver clock. A low-cost GNSS receiver normally uses a crystal oscillator as its clock, and this leads to a large receiver clock error. Therefore, the receiver clock error has to be treated as an unknown alongside three position unknowns. In open areas, the number of fault-free GNSS observations is significantly larger than 4, and the unknowns can be estimated accurately. However, in urban canyons, the majority of GNSS signals are obstructed by buildings, and lots of observations containing the positive NLOS errors are obtained. Under this situation, the receiver clock error estimation can absorb the common NLOS errors, complicating the differentiation between measurement errors and

the receiver clock error. This challenge severely affects the performance of GNSS FDE in urban canyons, degrading the positioning accuracy.

Figure 2 illustrates the challenge of GNSS FDE in urban canyons. As shown, the observations from satellites A, B, C and D are fault free, while these from E, F, G, H and I include NLOS errors. Different receiver clock errors can be estimated with different subsets of observations. As shown, the green circle represents the true receiver clock error estimated from the subset of 4 fault-free observations, while the yellow one denotes the wrong receiver clock error that is estimated from the subset of 5 faulty observations. Under this situation, the conventional FDE algorithm will lead to the solution from 5 faulty observations because it has a larger number of consistent measurements.

Figure 3 illustrates an example of GNSS search results in urban canyons. In this scenario, GNSS measurements were collected at a known location within the urban canyon, and a grid of points was generated around the true location. The number of consistent GNSS measurements at these grid points was evaluated and is represented using different colors. As depicted, the yellow points indicate the highest level of consistency. However, these yellow points are dispersed over a large area, predominantly in the cross-street direction, making it challenging to identify the correct points in this situation. For this example, the conventional method will inevitably cause the positioning errors as large as tens of meters. Other constraints are anticipated to control GNSS errors.

The motivation of this study is to model the receiver clock error accurately, which promisingly enhances urban GNSS positioning in two significant ways: (1) reduction of the number of GNSS unknowns; and (2) the improved GNSS FDE performance with the aid of the accurate information about the receiver clock error.

Different types of clocks can be used in GNSS receivers. The atomic clock is one of the most precise and stable clocks that are based on atomic transition frequencies. Their time accuracy can be on the order of 10^{-18} seconds. However, the high cost, large size, high power consumption, and complex maintenance requirements of traditional atomic clocks limit their widespread use in many practical applications. With technological advancements, CSACs have seen significant development over the past decade. They offer significant advantages in size, accuracy, stability, and energy consumption. Recently, the cost of CSACs has been reduced significantly. These advantages open opportunities for accurate GNSS positioning in urban canyons.

A test is conducted in an open area to compare the performance of CSAC with that of the normal Temperature Compensated Crystal Oscillator (TCXO). Figure 4 shows the setup of the hardware in the test. As shown, a splitter

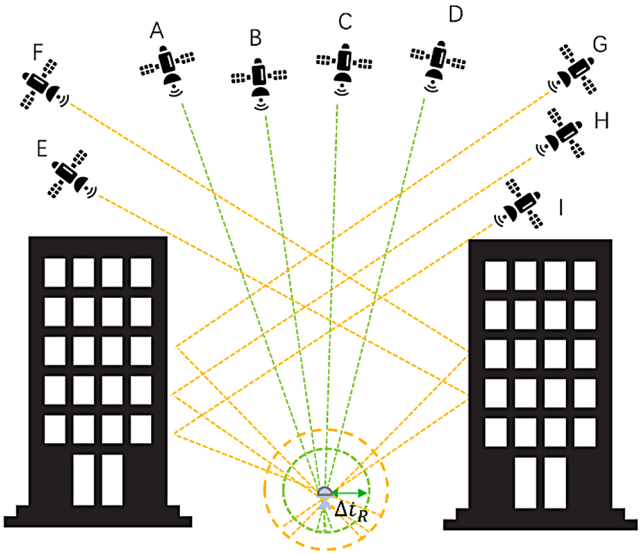

Fig. 2 Challenge of GNSS FDE in urban canyons

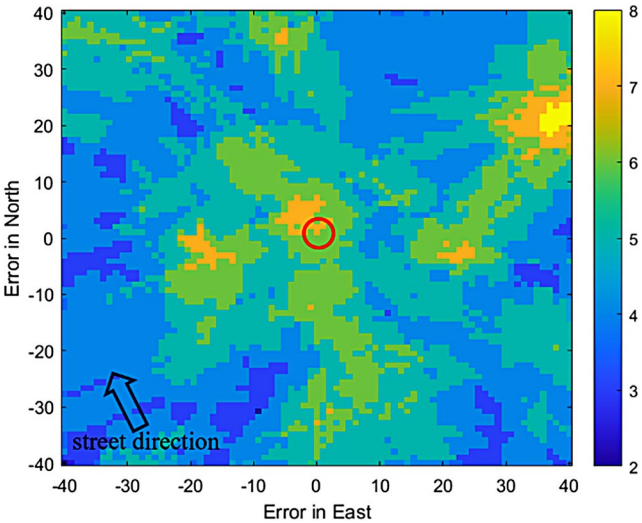

Fig. 3 The number of consistent GNSS measurements at grid points in urban canyons

divides GNSS signals into two Septentrio PolaRx5 receivers. The receiver in the red box uses TCXO as its own clock, while the receiver in the green box uses the external CSAC as its clock. In this study, the MAC-SA55 was used as the external CSAC, as shown in the green circle. The data collection took place on the rooftop of Block Z at The Hong Kong Polytechnic University, where the receivers had a clear view of over 40 satellites.

The receiver clock errors for two receivers were estimated by employing the standard point positioning technique. As depicted in Fig. 5, the analysis of the clock errors reveals that the CSAC error exhibited a drift of 25 m over a one-hour period, whereas the TCXO's clock error experienced a significantly larger drift, exceeding 6 km. This comparison

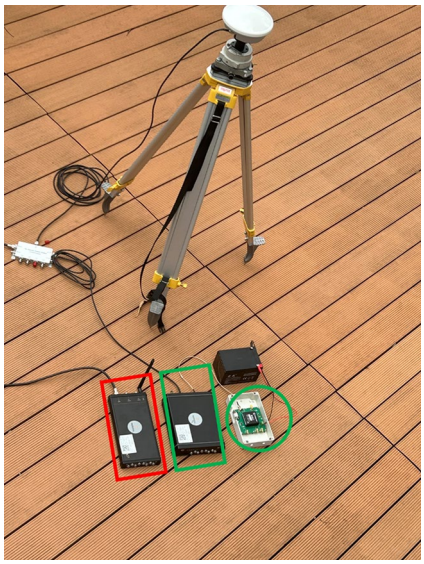

Fig. 4 Setup of GNSS receivers

underscores the superior stability and lower drift of CSAC compared to TCXO.

It seems from Fig. 5 that both receiver clock errors change linearly with time. Therefore, we will fit the receiver clock errors to a straight line

$$\Delta t_R(t) = at + b \tag{4}$$

where Δt_R denotes the receiver clock error; t represents time; b is the receiver clock bias; and a is the change rate of the receiver clock error. In the test, we fitted the receiver clock errors in the first five minutes to the line in Eq. (4). Two parameters are estimated: the bias b and the change rate a. In the following one hour, the receiver clock errors are predicted using the model. Figure 5 shows differences between the predicted errors and the true ones. It is shown that the CSAC errors can be estimated accurately with the simple model, achieving an RMSE of 1.01 m over an hour. In contrast, the accuracy of the predicted TCXO clock error rapidly deteriorates over time, with the largest errors being larger than 150 m within 1 h. It can be concluded from Fig. 6 that the CSAC error can be modeled accurately and easily. Therefore, in this study, the CSAC will be used as the clock for the GNSS receiver, and the constraints of the receiver clock error will be exploited to improve the GNSS FDE performance.

GNSS FDE with the aid of an urban map and a CSAC

In this study, a novel FDE algorithm is developed with the aid of a CSAC and an urban map. Figure 7 presents the flowchart of this algorithm. As depicted, the CSAC errors are predicted, which are in turn applied in GNSS solutions. Then, a number of candidate points are generated on the 3D urban map. The height information derived from the map is further used to constrain GNSS positions. Finally, each candidate point undergoes an assessment to determine the one that yields the highest degree of consistency, under the constraints of height and receiver clock error. These steps will be described in detail in this section.

Modelling CSAC error

As discussed in the previous section, CSAC has a high frequency stability, enabling accurate predictions within the time domain. To construct an accurate CSAC error model, it is important to acquire high-quality CSAC error data over a specific duration. In scenarios where the user remains in urban environments for extended periods, the CSAC errors may include outliers that need to be excluded. The proposed

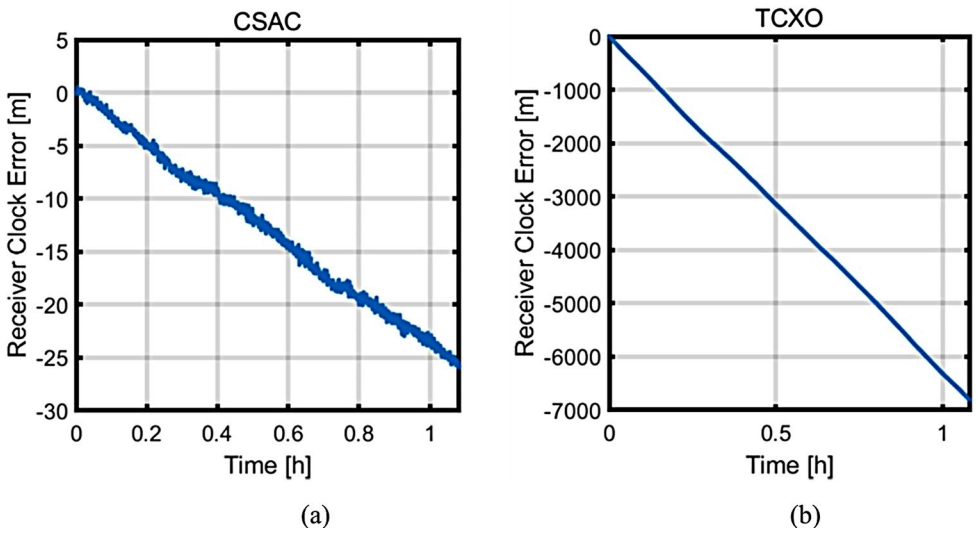

Fig. 5 Comparison of CSAC and TCXO clock errors

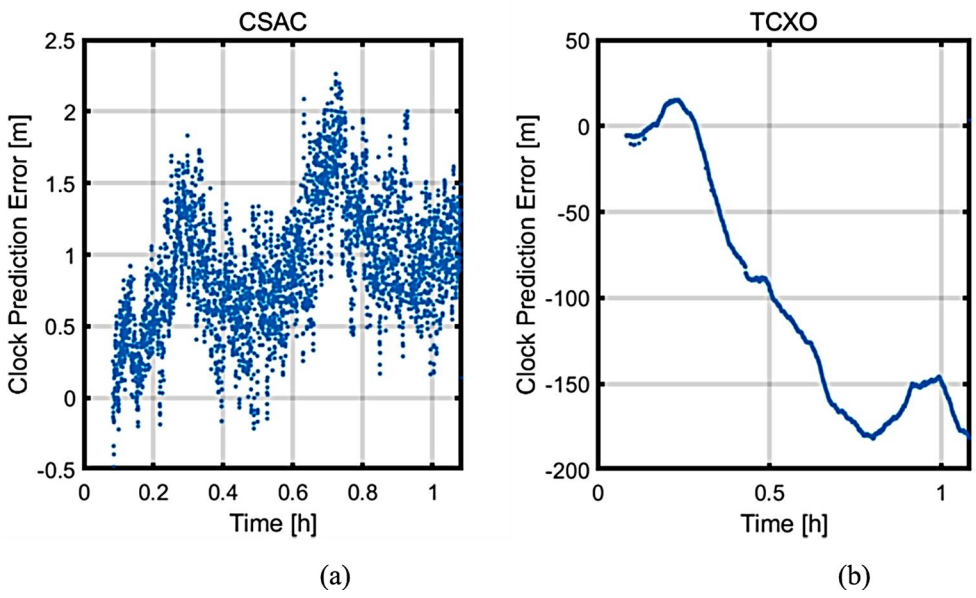

Fig. 6 Clock prediction error for: (**a**) CSAC and (**b**) TCXO

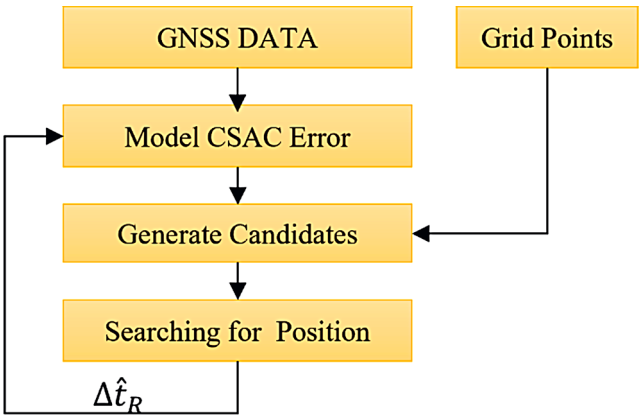

Fig. 7 Flowchart of the new GNSS FDE algorithm

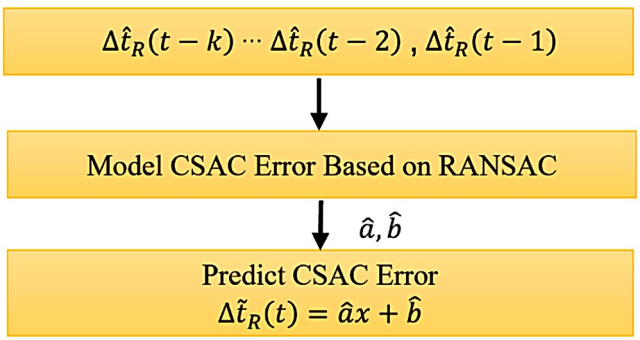

Fig. 8 CSAC error modeling and prediction

method involves robust modeling of CSAC errors by incorporating the most recent data.

Figure 8 shows the process of real-time modeling of the CSAC error. As shown, the receiver clock error is modeled using the estimates of the most recent k epochs: $\Delta\,\widehat{t}_R\,(t-k)\,,\ \Delta\,\widehat{t}_R\,(t-k+1)\,,\ldots\,,\Delta\,\widehat{t}_R\,(t-1)$. The Random Sample Consensus (RANSAC) algorithm is employed to estimate the two parameters based on the these CSAC error data. A subset comprising of two data points is selected from the dataset of CSAC errors to estimate the two parameters a and b. All data points in the entire dataset are evaluated against the modeled errors. A CSAC error is classified as an outlier, or an inlier based on the magnitude of difference. This iterative process continues until a sufficiently large number of inliers is established. Ultimately, the robust parameter estimates $\widehat{a}$ and $\widehat{b}$ obtained through the RANSAC method are used to predict the receiver clock bias $\Delta\,\widetilde{t}_R\,(t)$ at the current time t. The predicted CSAC error will be used later to correct the receiver clock error.

Generation of candidate points on the urban map

As discussed, the majority of GNSS observations are contaminated by NLOS or multipath errors in urban canyons. Under this situation, the reliable FDE is particularly difficult, posing a challenge for estimating four GNSS unknowns. In addition to CSAC clock, the urban map provides information on the height of the user position. In this study, the urban map will be used to generate the candidates, constraining GNSS heights. More importantly, the indoor space is excluded from the potential candidates since we know that users are in the outdoor environment.

We will firstly estimate an initial GNSS position using the residual based GNSS algorithm. The local coordinate of the initial position is given by $\boldsymbol{p}_0(e_0, n_0)$. We will then find generate a number of grid points within a circle centered at the initial position, with a radius of R. Suppose that the grid points searched are represented as $\boldsymbol{p}_i = (e_i, n_i)$ where $i = 1,\ 2,\ 3\ldots\ I$ and I is the number of candidate points.

The differences between the searched grid points with the initial position is given by

$$\Delta \boldsymbol{p}_i = \boldsymbol{p}_i - \boldsymbol{p}_0 = (\Delta e_i, \Delta n_i) \tag{5}$$

In the next subsection, the evaluation will be performed to search for the optimal point from the I candidate points.

Figure 9 illustrates the process of candidate generation through the urban map. The candidate points, marked in red, are selected from grid points through a circle centered at the initial point $\boldsymbol{p}_0$, which is marked as a green triangle in the figure. As shown, the grid points are generated in outdoor areas with a spacing of 2 m. When the indoor area is considered, the number of candidate points is around 1200. In this study, the indoor area is excluded, and this number is reduced to around 600. It should be noted that the search region should be large enough to encompass the true position. In this study, the largest initial positioning error will be evaluated to determine the search radius.

The conventional consistency checking methods try to check all the subsets of measurements. Different from previous methods, we will evaluate all the candidate points, and search for the position that agrees with the measurements. Specifically, we will simulate the measurements at each candidate point based on the real measurements. The consistency of the simulated measurements will be evaluated, and then the point that leads to the best consistency is regarded as the solution. Details of the method will be presented in the next subsection.

Searching for GNSS positions

As discussed, the constraints of the receiver clock and the height can be derived from the CSAC error model and the city map, respectively. In this section, we will search for the position under constraints of both the height and the receiver clock.

The city map is represented using a local coordinate system. Therefore, we need to transfer the WGS84 coordinate system to a local coordinate system first. The relation between the WGS-84 and the local coordinate system can be represented by

$$\boldsymbol{x} = \boldsymbol{R}\boldsymbol{x}' \tag{6}$$

where the unknown $\boldsymbol{x}' = [\Delta e, \Delta n, \Delta h, \Delta t_R]^T$ in the local coordinate system; $\boldsymbol{R}$ is the conversion matrix.

Applying (6) into (1) gives the following Eq.

$$\boldsymbol{l} = \boldsymbol{A}\boldsymbol{R}\boldsymbol{x}' + \boldsymbol{\epsilon} \tag{7}$$

The scalar form of the above equation can be represented as follows

$$l^s = a_e^s \Delta e + a_n^s \Delta n + a_u^s \Delta u + \Delta t_R + \epsilon^s \tag{8}$$

where $(a_e^s, a_n^s, a_u^s, 1)$ is the s-throw in the matrix $\boldsymbol{AR}$.

In this study, the height component Δu is derived from the city map, while the receiver clock error $\Delta \tilde{t}_R$ is predicted using the model. The details were described in the

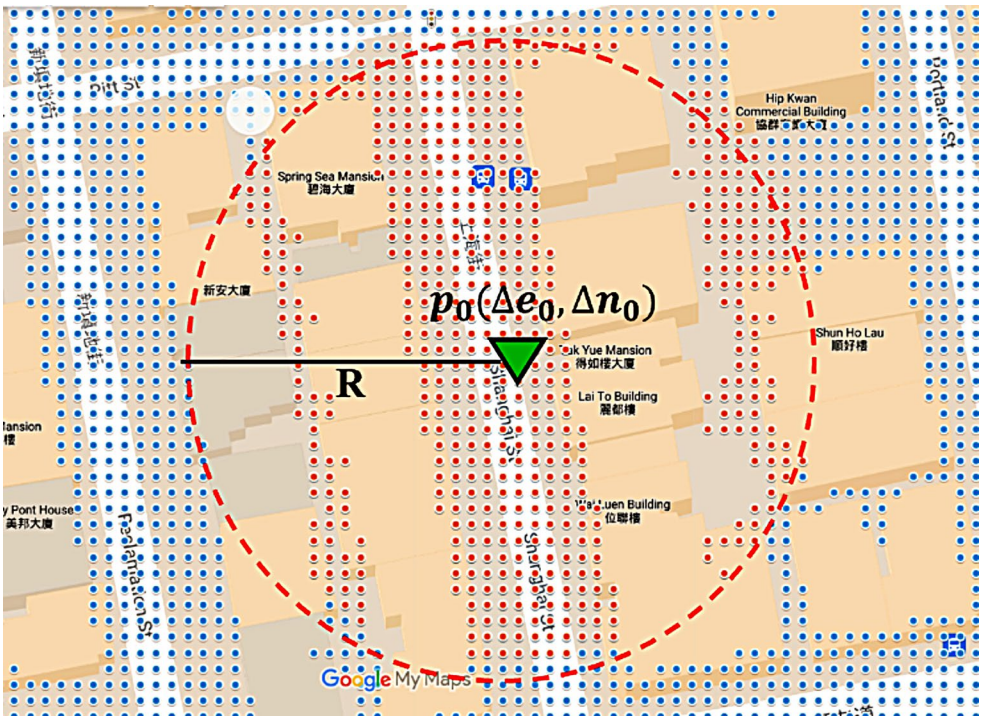

Fig. 9 Example of generating candidate points

previous two subsections. Equation (8) can therefore be rearranged as

$$m^s = l^s - \Delta\ \widetilde{t}_R - a_u^s \Delta u = a_e^s \Delta e + a_n^s \Delta n + \epsilon^s \tag{9}$$

where $m^s = l^s - \Delta\ \widetilde{t}_R - a_u^s \Delta u; a_e^s$、$a_n^s$ and a_u^s denote the known parameters for satellite s; Δe and Δn are two position unknowns. It can be seen from (9) that the number of unknowns in GNSS was reduced from 4 to 2. The slope-intercept form of Eq. (9) is given as follows

$$z^s = y^s \Delta e + \Delta n \tag{10}$$

where $z^s = \frac{m^s}{a_n^s}; y^s = \frac{a_e^s}{a_n^s}$; $s = 1,2\ldots.,n$. It can be seen that z^s and y^s are known coefficients, while Δe and Δn are the slope and the intercept that should be determined.

GNSS measurements in Eq. (11) are often affected by multiple simultaneous outliers. In this study, the Hough transform estimator is employed to find the most consistent measurements. The Hough transform is a robust technique for detecting simple geometric shapes in images, even in the presence of many outliers. It works by converting the observation space into the parameter space, making it easier to detect outliers. The parameter space can be derived from Eq. (11), and written as follows:

$$\Delta n = z^s - y^s \Delta e \tag{11}$$

where Δn and Δe are two unknowns. The Hough Transform technique tries to estimate the unknowns by finding the maximum number of intersections.

We will use an example in Fig. 10 to illustrate how to estimate the unknowns based on Hough Transform. In Fig. 10 (a), different satellites are represented as distinct points (y^s, z^s) in the 2D observation space. In this example, there are five fault-free measurements (green dots) and three faulty measurements (yellow dots). Identifying collinear points is essential to estimate the two unknowns: Δe and Δn. The observation space in Fig. 10 (a) is then mapped to the parameter space, as illustrated in Fig. 9 (b). As shown, the five collinear points in Fig. 10 (a) are represented by five lines that intersect around a point. The intersection of these lines is in fact the real position (Δe, Δn). To find the point that results in the maximum number of intersections, the parameter space is discretized into cells, which are shown as blocks in Fig. 10 (b). The block including the largest number of lines is selected as the final solution.

We will search for the Hough Transform solution by using the candidate points $\Delta \boldsymbol{p}_i = (\Delta e_i, \Delta n_i)$, which are generated in the previous subsection. For each candidate $\Delta \boldsymbol{p}_i = (\Delta e_i, \Delta n_i)$, where $i = 1, 2, \ldots I$, the number of lines in that cell is counted as $Count(\Delta e_i, \Delta n_i)$. Hough Transform determines the maximum number of consistent measurements

$$MaxN = \underset{(\Delta e_i, \Delta n_i)}{argmax}\, Count(\Delta e_i, \Delta n_i) \tag{12}$$

As shown, the position that corresponds to this maximum number of consistent measurements is considered the final solution of the algorithm. The receiver clock error will be estimated. Suppose that the searched subset of consistent measurements is denoted as Q. The receiver clock error is estimated as follows:

$$\Delta \widehat{t}_R = \Delta\ \widetilde{t}_R + 1/MaxN \sum\nolimits_{s \in Q} m^s \tag{13}$$

Finally, this estimated receiver clock error is stored in the memory, which will be used to predict the receiver clock error in the next epoch.

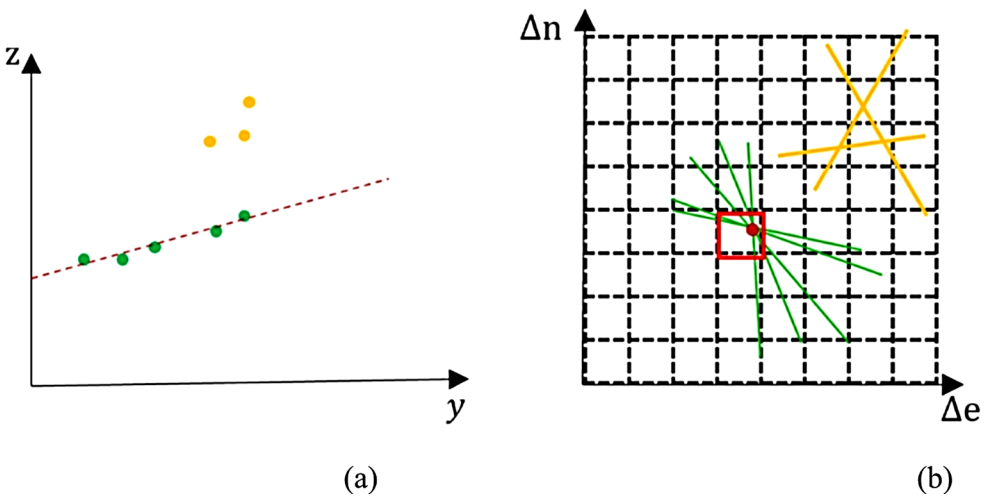

Fig. 10 Illustration of Hough Transform: (**a**) observation space and (**b**) the parameter space

(a) (b)

Fig. 11 Testing points: (**a**) eight lampposts used in the test; and (**b**) testing conditions

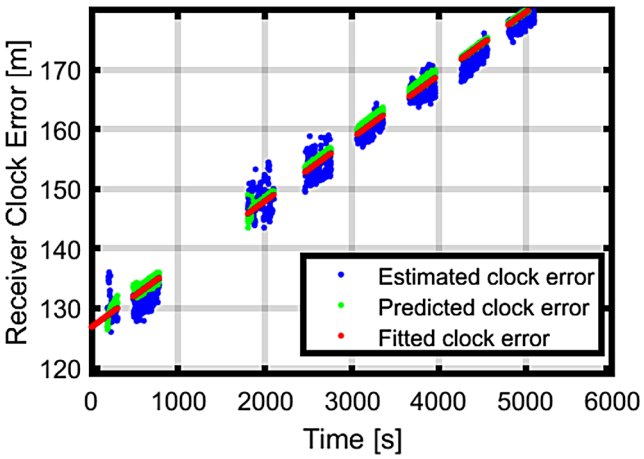

Fig. 12 The estimated receiver clock error and the predicted receiver clock error

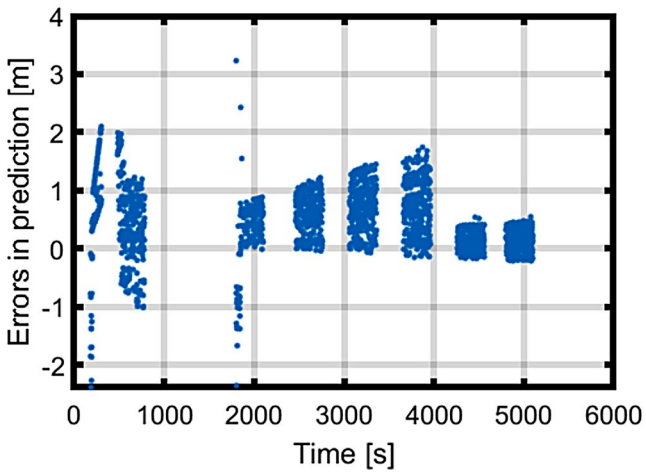

Fig. 13 Accuracy evaluation of the CSAC error prediction

Performance evaluation

Extensive tests were conducted in urban canyons in Hong Kong. Figure 11 shows the testing environments. As shown, the tests were performed near eight lampposts. The position coordinates of these lampposts had been precisely surveyed and were supplied by the Lands Department of Hong Kong. At each lamppost, five minutes of GNSS data collected using a Septentrio receiver, which was disciplined by a CSAC. The model of the CSAC used in this study is MAC-SA55.

Figure 12 shows the estimated receiver clock error in blue dots, which are estimated using Eq. (13). At each epoch, the receiver clock error is predicted using the RANSAC method based on the estimated receiver clock errors in most recent k epochs ($k = 1800$). In real time applications, it is not acceptable to derive the first position by waiting for 1800 s. In this study, we started to predict the receiver clock error with data of 2 min. In Fig. 11, the predicted receiver clock errors are shown as orange dots. To evaluate the performance of the predicted receiver clock error, we fitted the receiver clock error during the whole test to a simple linear model. In Fig. 12, the fitted clock errors are shown as red dots. The comparison between the orange dots and the red dots showed that the receiver clock error can be predicted accurately using the RANSAC method in this study.

We used the fitted receiver clock errors to evaluate the performance of the prediction. Figure 13 shows that the CSAC errors can be predicted accurately using the proposed RASAC method. However, in the beginning of the

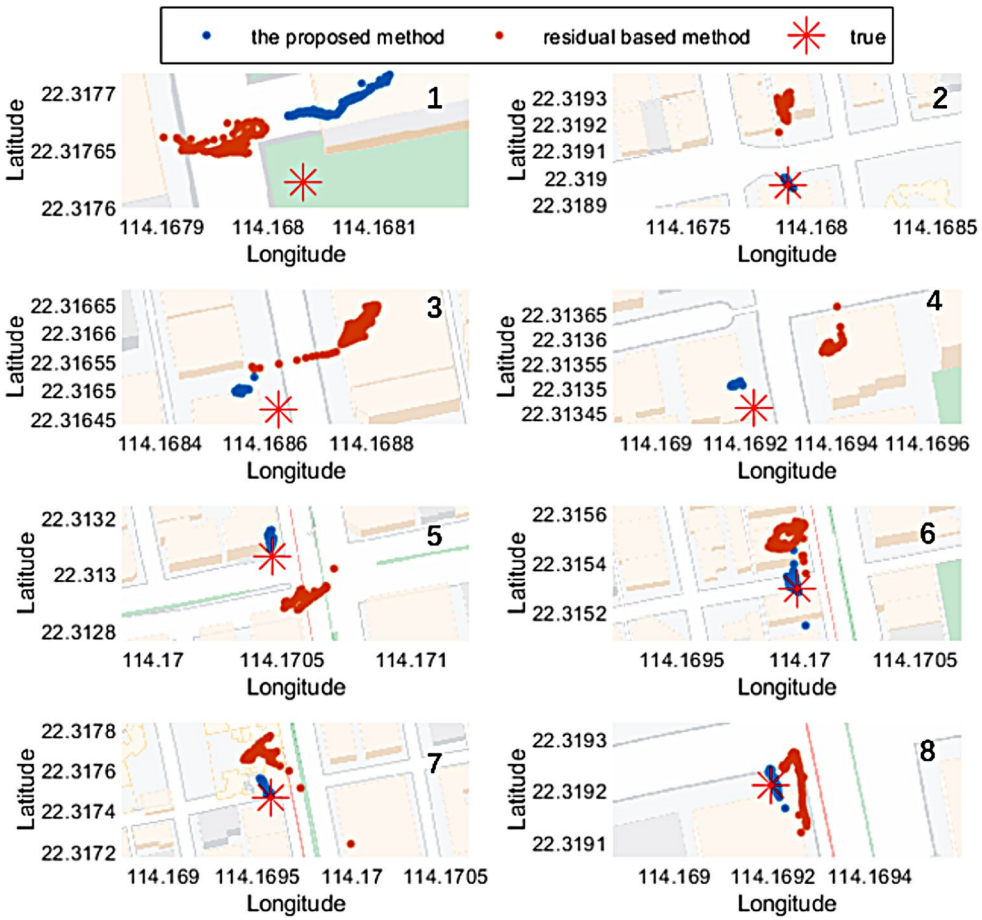

Fig. 14 Positions delivered by the residual based FDE and the proposed method for eight points

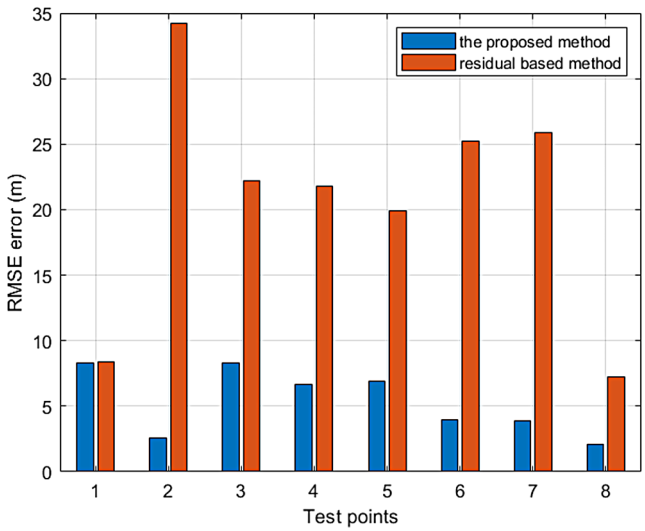

Fig. 15 Comparison of RMS errors between the residual based FDE and the proposed method

prediction, the prediction errors are as large as 4 m. This is caused by the lack of enough data about the clock errors in the beginning. As shown, when there are sufficient data, the prediction errors were reduced immediately.

We also searched for positions using the Hough Transform method, under constraints of height and receiver clock. Figure 14 compares the results from the conventional residual based algorithm and these from the proposed algorithm. As shown, large errors were caused in solutions from the conventional method. In addition, out of a total of 2400 epochs for calculation, the traditional FDE method failed in 500 epochs, whereas the new method successfully computed all epochs. More importantly, the positioning accuracy was significantly improved if the new method is applied.

Figure 15 shows the positioning accuracy of the proposed method and that of the conventional method. As shown, the GNSS accuracy of the conventional method was 20.6 m, while that of the proposed method has been reduced to 5.3 m.

To assess the robustness and performance of the proposed GNSS FDE algorithm under dynamic conditions, we performed dynamic experiments in Mong Kok, Hong Kong on 20 August 2024. As shown in Fig. 16, the Septentrio receiver with an external MAC-SA55 was installed inside the vehicle, while the GNSS antenna was mounted on the vehicle's roof along the central axis.

During the test, the vehicle traveled along four main streets in a counterclockwise direction, and the trajectories

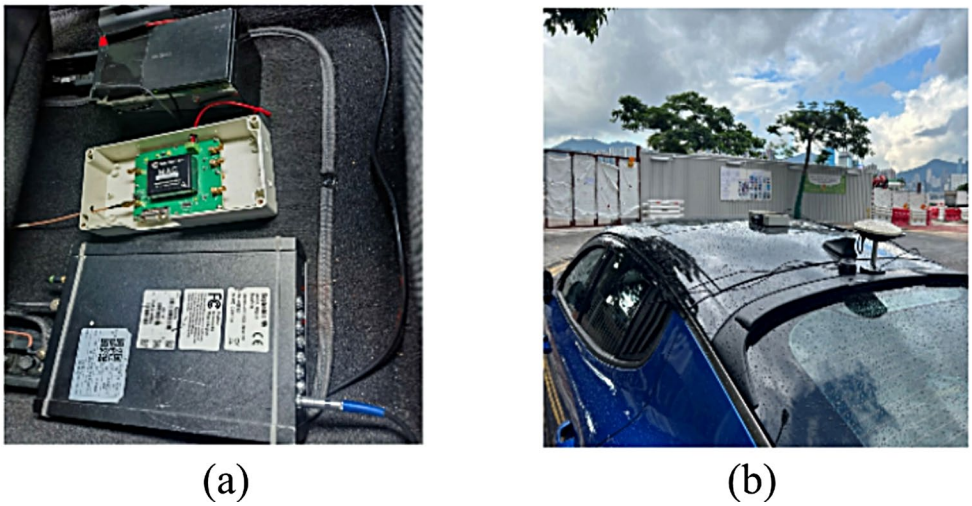

Fig. 16 Setup of the dynamic test: (**a**) the Septentrio receiver with an external MAC-SA55; and (**b**) GNSS antenna

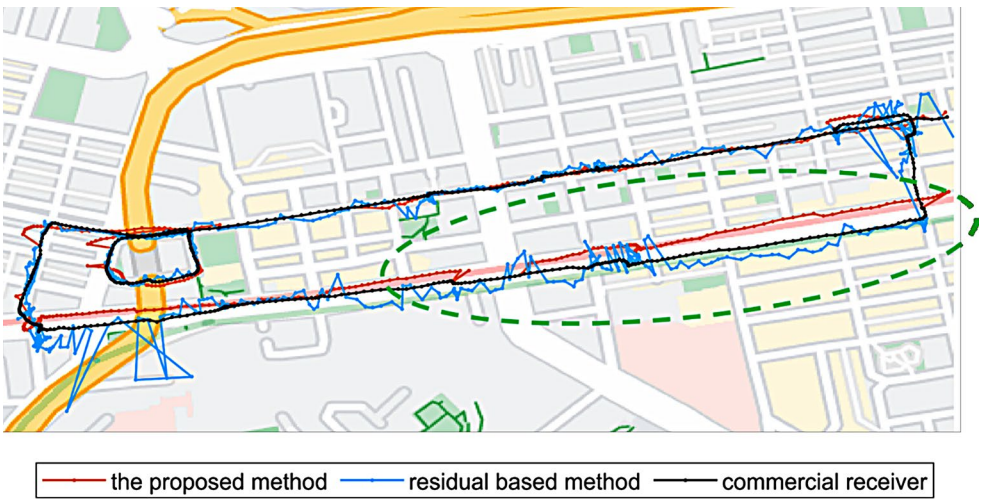

Fig. 17 Comparison of vehicle trajectories using different methods

derived from different methods were projected onto the map, as shown in Fig. 17. The blue line is calculated using the residual-based method, the black line is derived from the commercial receiver, and the orange line is computed using the proposed method. It can be concluded that the proposed method is more close to the real trajectory, compared with other methods. As shown in the green oval, the errors in positions from the commercial receiver can be as large as 20 m, while the meter-level positioning is achieved by using the proposed method.

The main differences among the three results in Fig. 17 appear on Street 3, identified as Nathan Road, a bidirectional three-lane street. During the test, the vehicle mainly remained in the second lane from the left. As shown in Fig. 17, the positioning accuracy of the proposed method on Nathan Road is significantly better than both the residual-based method and the survey-grade receiver results. To further evaluate accuracy, the centerline of the second lane was used as a reference, and the root mean square error (RMSE) in the cross-street direction for all three methods was calculated, as shown in Fig. 18. The results show that the proposed method achieves a significantly lower RMSE compared to both the survey-grade GNSS position and the residual-based method. Specifically, the proposed method exhibits an RMSE of approximately 7 m, which is markedly lower than the RMSE of the survey-grade GNSS position at approximately 15 m and the residual-based method at around 22 m.

Conclusions

This paper proposed a novel FDE method that leverages CSAC and city map constraints to achieve stable and reliable positioning services in urban canyons. The algorithm reduces the number of positioning parameters from four to two by applying constraints on height and receiver clock. With these constraints, we developed a new FDE algorithm based on Hough Transform. The extensive tests conducted in the urban canyons of Hong Kong demonstrated the

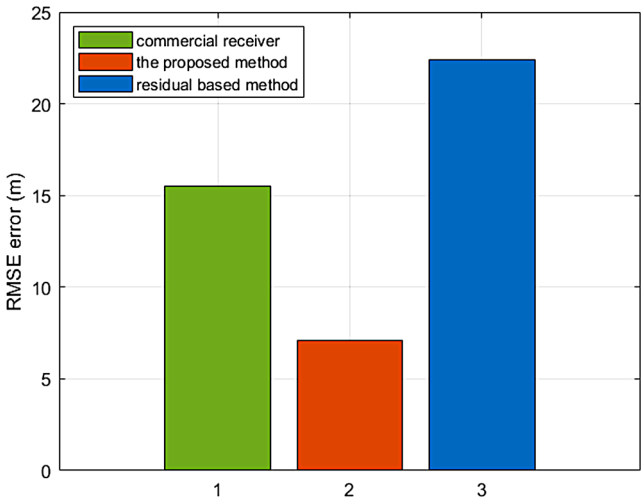

Fig. 18 Comparative analysis of cross-street RMSE for different positioning methods on nathan road

effectiveness of the proposed method. The results showed a significant improvement in positioning accuracy, reducing errors from 20 m to less than 6 m with the new approach. Furthermore, the new algorithm successfully computed positions in all test epochs, whereas the traditional FDE method failed in 500 out of 2400 epochs. This demonstrates that integrating CSAC and city map provides a robust solution for GNSS positioning in complex urban environments, effectively addressing the challenges of signal obstruction and multipath effects.

Acknowledgements This study was funded by the Open Fund from the State Key Laboratory of Satellite Navigation System and Equipment Technology (grants no. CEPNT2022A02 and SCX2168X008).

Author contributions Y.M. and D.W., Conceptualization, Methodology, Writing original draft; W.C., C.Y., and Z.H., Software, Reviewing and Editing.

Funding Open access funding provided by The Hong Kong Polytechnic University

Data availability The datasets generated and analyzed during the current study are available from the corresponding author upon reasonable request.

Declarations

Ethical approval Not applicable.

Competing interests The authors declare no competing interests.

References

Cash P, Krzewick W, Machado P, Overstreet KR, Silveira M, Stanczyk M, Taylor D, Zhang X(2018) Microsemi chip scale atomic clock (CSAC) technical status, applications, and future plans. In: 2018, Frequency E, Forum T (EFTF). IEEE, pp. 65–71

Dirksen M, Ronda RJ, Theeuwes NE, Pagani GA (2019) Sky view factor calculations and its application in urban heat island studies. Urban climate, 30. https://doi.org/10.1016/j.uclim.2019.100498

Groves PD (2011) Shadow matching: a new GNSS positioning technique for urban canyons. J Navig 64:417–430

Groves PD, Adjrad M (2019) Performance assessment of 3D-mapping–aided GNSS part 1: algorithms, user equipment, and review. Navigation 66:341–362

Hsu L-T, Gu Y, Huang Y, Kamijo S (2016) Urban Pedestrian Navigation using smartphone-based Dead reckoning and 3-D map-aided GNSS. IEEE Sens J 16:1281–1293. https://doi.org/10.1109/jsen.2015.2496621

Hsu L-T, Tokura H, Kubo N, Gu Y, Kamijo S (2017) Multiple Faulty GNSS Measurement Exclusion based on consistency check in Urban canyons. IEEE Sens J 17:1909–1917. https://doi.org/10.1109/jsen.2017.2654359

Krawinkel T, Schön S (2016) Benefits of receiver clock modeling in code-based GNSS navigation. GPS Solutions 20:687–701

Kunzi F, Montenbruck O (2023) Precise disciplining of a chip-scale atomic clock using PPP with broadcast ephemerides. GPS Solutions 27:165

Liu Q, Gao C, Xhafa A, Gao W, López-Salcedo JA, Seco-Granados G (2024) Performance analysis of GNSS + 5G hybrid positioning algorithms for smartphones in Urban environments. IEEE Trans Instrum Meas 73:1–9. https://doi.org/10.1109/tim.2023.3338677

Martinez GD, Li C, Staron A, Kitching J, Raman C, McGehee WR (2023) A chip-scale atomic beam clock. Nat Commun 14:3501. https://doi.org/10.1038/s41467-023-39166-1

Massarweh L, Fortunato M, Gioia C (2020) Assessment of real-time multipath detection with Android raw GNSS measurements by using a xiaomi mi 8 smartphone. In: 2020 IEEE/ION Position, Location and Navigation Symposium (PLANS). IEEE, pp. 1111–1122

Miao C, Yu S, Hu Y, Zhang H, He X, Chen W (2020) Review of methods used to estimate the sky view factor in urban street canyons. Build Environ. 16810.1016/j.buildenv.2019.106497

Ng HF, Zhang G, Luo Y, Hsu LT (2021b) Urban positioning: 3D mapping-aided GNSS using dual-frequency pseudorange measurements from smartphones. Navigation 68:727–749. https://doi.org/10.1002/navi.448

Sharma H, Bochkati M, Pany T (2019) Influence of the multipath mitigation on precise positioning with smartphone raw GNSS measurements. In: Proc. ISGNSS

Sheta A, Mohsen A, Sheta B, Hassan M (2018) Improved localization for Android smartphones based on integration of raw GNSS measurements and IMU sensors. In: 2018 International conference on computer and applications (ICCA). IEEE, pp. 297–302

Wang L, Groves PD, Ziebart MK (2013) Urban positioning on a smartphone: Real-time shadow matching using GNSS and 3D city models. Navigation

Wang L, Groves PD, Ziebart MK (2014) Smartphone Shadow Matching for Better Cross-street GNSS Positioning in Urban environments. J Navig 68:411–433. https://doi.org/10.1017/s0373463314000836

Wang J, Chen W, Weng D, Ding W, Li Y (2023) Barometer assisted smartphone localization for vehicle navigation in multilayer road networks. Measurement 211:112661

Weng D, Chen W, Lu Y, Ji S, Luo H, Cai M (2023a) Global DGNSS service for mobile positioning through public corrections. Adv Space Res 72:4402–4412

Weng D, Hou Z, Meng Y, Cai M, Chan Y (2023b) Characterization and mitigation of urban GNSS multipath effects on smartphones. Measurement 223:113766

Weng D, Chen W, Ji S, Wang J (2024) Intelligent Urban Positioning using smartphone-based GNSS and Pedestrian Network. IEEE Internet of Things Journal

Yan W, Bastos L, Magalhães A (2019) Performance assessment of the android smartphone's IMU in a GNSS/INS coupled navigation model. IEEE Access 7:171073–171083

Yao Y, Peng W, Xu C, Shi J, Cheng S, Ouyang C (2019) The realization and evaluation of mixed GPS/BDS PPP ambiguity resolution. J Geodesy 93:1283–1295

Yang Meng received the B.S. degree in Geomatics Engineering from North China University of Science and Technology in 2020, and the M.S. degree from China University of Geosciences (Beijing) in 2023. He is currently a Research Assistant with the Department of Land Surveying and Geo-Informatics, The Hong Kong Polytechnic University, Hong Kong. His research interests include GNSS, INS, multi-sensor fusion with visual data, and integrity monitoring of GNSS.

Duojie Weng received the B.S. and M.S. degrees in electrical engineering from Hohai University, Nanjing, China in 2007 and 2010, and the Ph.D. degree from The Hong Kong Polytechnic University, Hong Kong, in 2016. He is currently a Research Assistant Professor with the Department of Land Surveying and Geo-Informatics, The Hong Kong Polytechnic University, Hong Kong. His research interests include urban positioning, integrity monitoring of GNSS, Kinematic GPS, sensor integration for various navigation systems.

Cheng Yang received a Ph.D. degree in Department of Land Surveying and Geo-Informatics, at the Hong Kong Polytechnic University, Hong Kong, in 2017. He received the B.E. degree from Nanjing University of Aeronautics and Astronautics, Nanjing, China, in 2003 and the M.S. degree from The Hong Kong Polytechnic University, Hong Kong, in 2012. He is currently associate professor at China University of Geosciences Beijing. His research interest includes integrated navigation and GPS positioning.

Wu Chen received his Ph.D. degree from Newcastle University, Newcastle upon Tyne, UK, in 1992. He is currently a Professor with the Department of Land Surveying and Geo-Informatics, The Hong Kong Polytechnic University, Hong Kong. His current research interests include the GNSS positioning quality evaluation, system integrity, various GNSS applications, seamless positioning and SLAM.

Zhiyu Hou received the B.E. degree in Surveying and Mapping Engineering from Shandong University of Science and Technology, Qingdao, China, in 2022, and the M.S. degree from the Hong Kong Polytechnic University, Hong Kong, in 2023. He is currently a Research Assistant with the Department of Land Surveying and Geo-Informatics, The Hong Kong Polytechnic University, Hong Kong. He is currently a Research Assistant at the Department of Land Surveying and Geo-Informatics, Hong Kong Polytechnic University. His research interests include GNSS signal quality monitoring and interference detection, mitigating GNSS multipath effects in urban canyons for pedestrian navigation, and developing automotive lane-level navigation systems.